Friedrich-Schiller-Universität Jena

Physikalisch-Astronomische Fakultät

Helmholtz-Institut Jena

seit 1558

Angular and Polarisation Properties of Bremsstrahlung Radiation in the Short Wavelength Limit

Bachelorarbeit

zur Erlangung des Grades eines

Bachelor of Science

vorgelegt von

Robert Müller

geboren in Darmstadt

August 2013, Jena

Eigenständigkeitserklärung

Der Autor erklärt, die vorliegende Arbeit selbstständig und ohne Benutzung anderer als der angegebenen Hilfsmittel verfasst zu haben.
Die aus fremden Quellen direkt oder indirekt übernommenen Gedanken sind ausnahmslos als solche kenntlich gemacht. Die Arbeit ist in gleicher oder ähnlicher Form oder auszugsweise noch nicht im Rahmen einer anderen Prüfung vorgelegt worden.

Robert Müller

Diese Arbeit wurde betreut durch:
PD Dr. Andrey Surzhykov
(Erstkorrektur)
Prof. Dr. Stephan Fritzsche
(Zweitkorrektur)

Die dir zugemessene Zeit ist so kurz, dass du,
wenn du eine Sekunde verlierst, schon dein ganzes Leben verloren hast,
denn es ist nicht länger
es ist immer nur so lang wie die Zeit, die du verlierst.

Franz Kafka

Contents

1 Introduction

It is one of the elementary statements classical electrodynamics issue that accelerated charges emit radiation. One of the most famous examples is of course the Hertzian dipole from which Heinrich Rudolf Hertz discovered the existence of electromagnetic waves. One now expects also elementary particles emitting radiation when they are accelerated or decelerated. This effect was first used to generate X-rays by focusing an electron beam on an appropiate cathode material. The kinetic energy the electrons lose by hitting the surface of the cathode is emitted in form of X-rays. At least it was Arnold Sommerfeld in accordance with Wilhelm Conrad Röntgen who called this process *bremsstrahlung*.

Particularly there are two bremsstrahlung processes to be taken into account when considering the interaction of charged particles and atoms or ions. First of all there is so called ordinary or electron-atom bremsstrahlung. This process is responsible for the effects observed in the middle of the 20th century. As one can see in Fig. 1.1 ordinary bremsstrahlung is emitted by an electron scattered on the (screened) potential of an atom or ion.

Polarisation bremsstrahlung is caused by the atomic structure deformed by the passing electron. Thus a dipole moment is induced. Since this so called "polarisation" is time dependent it also emits radiation as illustrated in Fig. 1.2.

But why is it important to understand at least the process of electron-atom bremsstrahlung as thoroughly as possible? There are several answers. The properties of bremsstrahlung radiation strongly depend on the incident electron. In this context radiation measurements can be used for electron beam diagnostics for example to tell wether the incident electron is polarised and if so in which direction. This knowledge is for instance important for any experiment requiring polarised electron beams. It turned out that bremsstrahlung could also be a useful tool for plasma diagnostics. An atomic plasma includes free electrons as well as atomic nuclei. When electrons are scattered on the bare nuclei one can draw conclusions

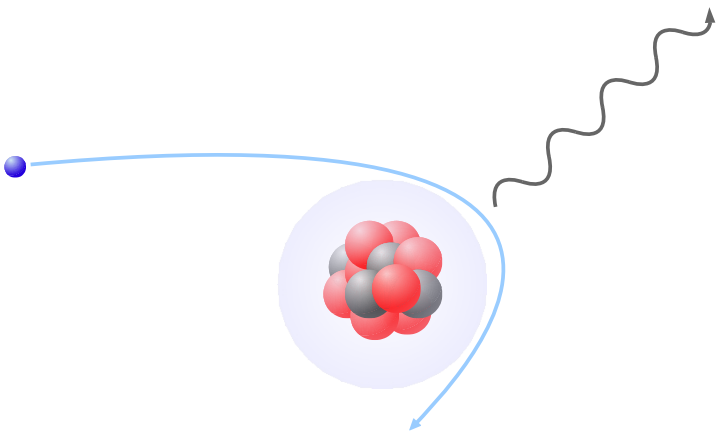

Figure 1.1: Principle of ordinary bremsstrahlung.

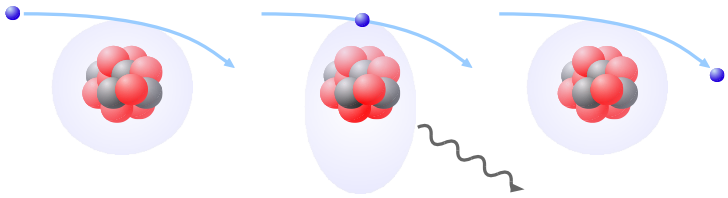

Figure 1.2: Principle of polarisation bremsstrahlung.

according to the plasma properties from observing the bremsstrahlung radiation emitted during that process. Since bremsstrahlung is emitted during every process including free electrons and atoms it often is a background effect which increases the noise level of the recorded data. That means the better the knowledge about the background effect is, in this case bremsstrahlung, the better one can distinguish the investigated effect from the rest of the data.

As the applications are so manifold, it is essential to have easy access to all bremsstrahlung radiation properties for any experimental setup. The methods usually used for bremsstrahlung calculations are rather pedestrian and inflexible. This means that in most cases new calculations are necessary for different observation angles as well as for different electron energies. The aim of this analysis is now to show up a way to provide this data in a way which makes it utilisable for as many applications as possible. To meet these demands the calculations have to be fast, the parameters may be chosen from a wide range and the data should be calculated with the same precision modern experimental measurements can achieve.

This work treats the *short wavelength limit* of electron-atom bremsstrahlung which means the electron transfers all its energy to the photon. Unless not defined otherwise we assume that the energy of the emitted photon equals the energy of the incoming electron.

All Expressions in this work are given in atomic units ($e = m_e = \hbar = 1$).

2 Dirac Wavefunctions and Matrix Elements

For the description of the bremsstrahlung process, solutions of the Dirac equation are used to describe the electrons. This way was chosen since a fully relativistic treatment of the electrons is necessary to cover a wide range of electron energies. For example an electron energy of 100 keV corresponds to a velocity of $v_e = 0.63c$ wich is already highly relativistic. In experiments energies of several hundred keV are more and more common during the continual growth of high energy physics. It is obvious that a relativistic treatment of the bremsstrahlung process is inevitable to describe the phenomena observed in modern physics.

2.1 Mathematical Preliminaries

This section covers not all mathemathics needed for the derivations done in this work. It should emphasise some important relations which are denotative for central steps.

2.1.1 Wigner D-function

The Wigner-D-functions performs a rotation of a state vector in the Hilbert space around the three Euler angles (α, β, γ). We label the rotated state vector with a tilde:

$$\widetilde{|jm\rangle} = \sum_{m'} D^{j}_{mm'}(\alpha,\beta,\gamma)\,|jm'\rangle \tag{2.1.1}$$

Important properties of this function can be found e.g. in Ref. [1]:

$$\left(D^{j_1}_{m_1 m_1'} \otimes D^{j_2}_{m_2 m_2'}\right)(\alpha,\beta,\gamma) = \sum_{jmm'} (j_1 m_1 j_2 m_2 | jm)(j_1 m_1' j_2 m_2' | jm') D^{j}_{mm'}(\alpha,\beta,\gamma) \tag{2.1.2a}$$

$$D^{j*}_{mm'}(\alpha,\beta,\gamma) = (-1)^{m-m'} D^{j}_{-m-m'}(\alpha,\beta,\gamma) \tag{2.1.2b}$$

$$D^{j}_{m0}(\alpha,\beta,\gamma) = \sqrt{\frac{4\pi}{2l+1}} \mathrm{Y}^{*}_{lm}(\beta,\alpha) = (-1)^{m} \sqrt{\frac{4\pi}{2l+1}} \mathrm{Y}_{l-m}(\beta,\alpha) \tag{2.1.2c}$$

2.1.2 Wigner-Eckart Theorem

The Wigner-Eckart theorem allows us to split any geometrical dependency from a matrix element. The result is the so called reduced matrix element which only depends on absolute

values not on projections. In a simplified form it reads with an arbitrary set of tensor operators A_{LM}:

$$\langle \alpha\, j' m' | A_{LM} | \alpha\, j m \rangle = \frac{(j m L M | j' m')}{\sqrt{2j+1}} \langle \alpha\, j' || A_L || \alpha\, j \rangle \tag{2.1.3}$$

In this representation the Wigner-Eckart theorem can be found in Ref. [2].

2.2 Dirac Equation

We are looking for the wavefunction of an relativistic electron in a stationary Coulomb field. Therefor we need to solve the Dirac eaquation for a single electron including a Coloumb potential

$$\left(-\mathrm{i}\hat{\boldsymbol{\alpha}}\,\mathrm{grad} + \hat{\beta} - \frac{Z}{r}\right) |\psi(\boldsymbol{r})\rangle = E\,|\psi(\boldsymbol{r})\rangle \tag{2.2.1}$$

where $\hat{\boldsymbol{\alpha}}$ is related to the Dirac matrices like $\hat{\alpha}^i = \hat{\beta}^{-1}\hat{\gamma}^i$ and $\hat{\gamma}^0 = \hat{\beta}$ and Z is the nuclear charge. In Equation (2.2.1) we neglected the size of the nucleus as well as any Breit or Hyperfine corrections. The eigenvalues of the Dirac Hamiltonian show up as shown in Fig. 2.1.

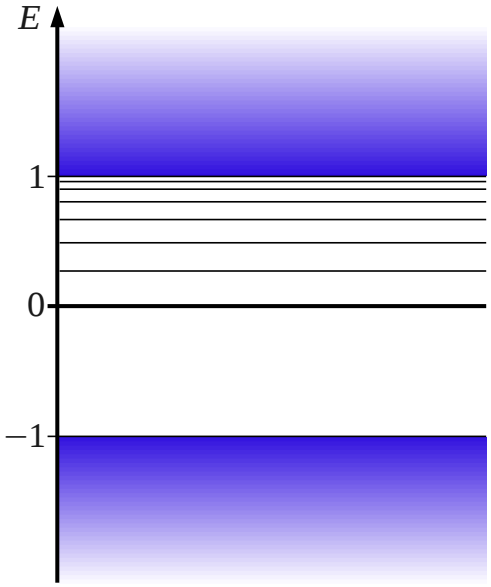

Figure 2.1: Illustration of the Dirac Hamiltonian eigenvalues.

From the Hamiltonian being Hermitician one can conclude that the $\hat{\boldsymbol{\alpha}}$-matrices as well as $\hat{\beta}$ have to be Hermitician too. We stipulate that the Dirac wavefunctions are also solutions of the Klein-Gordon equation. This yields additional relations between the $\hat{\boldsymbol{\alpha}}$ and $\hat{\beta}$ matrices. These equations can only be satisfyed by matrices having the minimal dimension 4×4 what fits nicely into a relativistic theory which at least requires four dimensional state vectors.

2.3 Dirac Wavefunctions

The Dirac equation does not allow a decomposition of the wavefunction in the form:

$$\psi_{nlm_l sm_s}(\boldsymbol{r}) = R_{nl}(r) \cdot \mathrm{Y}_{lm_l}(\vartheta\varphi) \cdot \chi_{sm_s}(\sigma) \tag{2.3.1}$$

This is because of the spin-orbit-coupling in the relativistic regime. Instead we can decompose the wavefunction into a radial and a spin-angular part since the total angular momentum operator $\hat{\boldsymbol{J}} = \hat{\boldsymbol{L}} + \hat{\boldsymbol{S}}$ commutes with the Dirac Hamiltonian. Usually Dirac wavefunctions are written as a two-spinor with two-spinors as its components

$$\psi_{\varepsilon\kappa m_j}(\boldsymbol{r}) = \begin{pmatrix} g_{\varepsilon\kappa}(r)\Omega_{\kappa m_j}(\hat{\boldsymbol{r}}) \\ \mathrm{i} f_{\varepsilon\kappa}(r)\Omega_{-\kappa m_j}(\hat{\boldsymbol{r}}) \end{pmatrix} \tag{2.3.2}$$

where ε is the energy of the particle, κ the relativistic quantum number and m_j the projection of the total angular momentum on the quantisation axis. The functions $g_{\varepsilon\kappa}(r)$ and $f_{\varepsilon\kappa}(r)$ describe the radial properties of the wavefunction, while $\Omega_{\pm\kappa m_j}(\hat{\boldsymbol{r}})$ contains its angular and spin dependencies. The angular functions are a tensor product of the spin wavefunction and the spherical harmonic which describes the angular behaviour.

$$\Omega_{\pm\kappa m_j}(\hat{\boldsymbol{r}}) = \sum_{m_l m_s} (l m_l \tfrac{1}{2} m_s | j m_j) \mathrm{Y}_{lm_l}(\hat{\boldsymbol{r}})\, \chi_{sm_s} \tag{2.3.3}$$

Since the spin wavefunction is a two-spinor itself the Dirac wavefunction is a four-spinor as claimed before. To obtain expressions for the radial components we follow Ref. [3]. By multiplying Eq. (2.3.2) with r, substituting $F(r) = r f(r)$ and $G(r) = r g(r)$ and inserting it into Eq. (2.2.1) one gets two coupled differential equations for the radial wavefunctions:

$$\left(\frac{\mathrm{d}}{\mathrm{d}r} - \frac{\kappa}{r}\right) F_{\varepsilon\kappa}(r) = \left(-E + \frac{Z}{r} + 1\right) G_{\varepsilon\kappa}(r) \tag{2.3.4a}$$

$$\left(\frac{\mathrm{d}}{\mathrm{d}r} - \frac{\kappa}{r}\right) G_{\varepsilon\kappa}(r) = \left(E - \frac{Z}{r} + 1\right) F_{\varepsilon\kappa}(r) \tag{2.3.4b}$$

The analytical solutions of these equations consist basically of the ${}_1\mathrm{F}_1$-Confluent Hypergeometric Function:

$$g_{\varepsilon\kappa}(r) = N_\kappa \sqrt{\varepsilon + 1}\,(2pr)^{s-1}\, \Re\left(\mathrm{e}^{-\mathrm{i}(pr+\delta_\kappa)}(s + \mathrm{i}\eta)\, {}_1\mathrm{F}_1(s + 1 + \mathrm{i}\eta, 2s + 1, 2\mathrm{i}pr)\right) \tag{2.3.5a}$$

$$f_{\varepsilon\kappa}(r) = -N_\kappa \sqrt{\varepsilon - 1}\,(2pr)^{s-1}\, \Im\left(\mathrm{e}^{-\mathrm{i}(pr+\delta_\kappa)}(s + \mathrm{i}\eta)\, {}_1\mathrm{F}_1(s + 1 + \mathrm{i}\eta, 2s + 1, 2\mathrm{i}pr)\right) \tag{2.3.5b}$$

Whith the electron momentum p, the phase δ_κ and the fine-structure constant α:

$$\zeta = \alpha \cdot Z \qquad s = \sqrt{\kappa^2 - \zeta^2} \qquad \eta = \frac{\zeta\varepsilon}{\kappa}$$

$$p = \sqrt{\varepsilon^2 - 1} \qquad e^{\mathrm{i}\delta_\kappa} = \sqrt{\frac{-\kappa + \mathrm{i}\eta/\varepsilon}{s + \mathrm{i}\eta}} \qquad N_\kappa = 2\sqrt{\frac{p}{\pi}} \frac{\left|\Gamma(s + \mathrm{i}\eta\right|}{\Gamma(2s+1)}\, \mathrm{e}^{\frac{1}{2}\pi\eta}$$

The wavefunction shown in Eq. (2.3.2) describes an electron in the continuum with a well defined total angular momentum and its projection.

However the experimentally accessible properties of electrons in the continuum are the asymptotic momentum and the projection of its spin on the quantisation axis. While the Schrödinger equation allows us to find closed expressions for a continuum electron with well defined asymptotic momentum by seperating it in parabolic coordinates we cannot find such expressions in the relativistic regime. Instead of a relativistic electron with well defined asymptotic momentum it is possible to perform an expansion in a plane wave and incoming and outgoing spherical waves whith well defined angular momentum and projection as shown in Eq. (2.3.2). This method also keeps the seperation into a radial and a spin-angular part. These incoming (+) and outgoing (−) waves can be derived directly from the Dirac equation. According to Ref. [3] they read:

$$\psi^{(\pm)}_{\varepsilon k_z m_s}(\boldsymbol{r}) = \sqrt{\frac{\pi}{2\varepsilon k}} \sum_{\kappa} \mathrm{i}^l \sqrt{4\pi(2l+1)}\, (l0\tfrac{1}{2}m_s|jm_s)\, \mathrm{e}^{\pm \mathrm{i}\Delta_\kappa} \psi_{\varepsilon\kappa m_j}(\boldsymbol{r}) \tag{2.3.6}$$

Here $\boldsymbol{k} = k_z$, $k = |\boldsymbol{k}|$ and the Coloumb phase shift $\Delta_\kappa = \delta_\kappa - \arg\left(\Gamma\left(s + \mathrm{i}\eta\right)\right) - \frac{1}{2}\pi s$. In Eq. (2.3.6) we considered the z-direction as the direction of the electron momentum as well as the quantisation axis. For the quantisation axis not coinciding with the direction of the electron momentum we keep the z-axis as the quantisation axis and rotate the space part of the wavefunction. Thus we obtain:

$$\psi^{(\pm)}_{\varepsilon \boldsymbol{k} m_s}(\boldsymbol{r}) = 4\pi \sqrt{\frac{\pi}{2\varepsilon k}} \sum_{\kappa m_j} \mathrm{i}^l \sqrt{4\pi(2l+1)}\, (l m_l \tfrac{1}{2} m_s|jm_s)\, \mathrm{e}^{\pm \mathrm{i}\Delta_\kappa} \mathrm{Y}^*_{l m_l}(\vartheta\varphi) \psi_{\varepsilon\kappa m_j}(\boldsymbol{r}) \tag{2.3.7}$$

In this case, where the quantisation axis is still the z-axis according to Eq. (2.1.2c) the spatial rotation reduces to a spherical harmonic function. Because of the spin projection not having a sharp value if quantisation and propagation axis are not the same this expression can only be used if a summation over the spin projection is performed.

2.4 Photon Interaction Operator

The emission of a photon during the bremsstrahlung process corresponds to a coupling to an external electromagnetic field within the Hamilton formalism. The interaction operator is:

$$\hat{H}_{\mathrm{int}} = \hat{\boldsymbol{\alpha}} \cdot \boldsymbol{A} \tag{2.4.1}$$

Here $\boldsymbol{A}$ is the vectorpotential. With $\operatorname{div} \boldsymbol{A} = 0$ (Coloumb gauge) one obtains

$$\boldsymbol{A}(\boldsymbol{r}) = \boldsymbol{u}^*_\lambda \, \mathrm{e}^{\mathrm{i}\boldsymbol{k}\boldsymbol{r}} \tag{2.4.2}$$

where $\boldsymbol{u}_\lambda$ is the unit polarisation and $\boldsymbol{k}$ the wave vector with the helicity $\lambda = \pm 1$ for either left or right circular polarisation (see Ref. [2]). Throughout this work we define:

$$\boldsymbol{u}_{\pm 1} = \frac{1}{\sqrt{2}}(u_x \pm u_y) \tag{2.4.3}$$

In order to get an expression for an arbitrary direction of the emitted photon we follow Rose [2] and perform a multipole or Rayleigh expansion. After that the vector potential can be written as follows:

$$\boldsymbol{A}(\boldsymbol{r}) = \sqrt{2\pi} \sum_{LMp} \mathrm{i}^L (2L+1)^{\frac{1}{2}} \mathrm{D}^L_{M\lambda}(\vartheta\varphi)\, (\mathrm{i}\lambda)^p \, \boldsymbol{a}^{(p)}_{LM}(\boldsymbol{r}) \tag{2.4.4}$$

The Wigner rotation matrix $D^L_{M\lambda}$ was introduced in Sec. 2.1. The field vectors, indexed by $p \in \{0,1\}$ can be found as

$$\boldsymbol{a}^{(0)}_{LM}(\boldsymbol{r}) = \mathrm{j}_L(kr)\boldsymbol{T}^M_{LL}(\vartheta\varphi) \tag{2.4.5a}$$

$$\boldsymbol{a}^{(1)}_{LM}(\boldsymbol{r}) = \mathrm{j}_{L-1}(kr)\left(\frac{L+1}{2L+1}\right)^{\frac{1}{2}}\boldsymbol{T}^M_{LL-1}(\vartheta\varphi) - \mathrm{j}_{L+1}(kr)(\frac{L}{2L+1})^{\frac{1}{2}}\boldsymbol{T}^M_{LL+1}(\vartheta\varphi) \tag{2.4.5b}$$

where j_L are spherical Bessel functions and $\boldsymbol{T}^M_{LL}$ vector spherical harmonics. We now have an expression for the interaction operator describing a photon emitted in an arbitrary direction which is additionaly separated into an angular and a radial part.

2.5 Reduced Matrix Elements

Using the results derived in the previous sections, we can now apply first order time-dependent pertubation theory. In this case the transition matrix is using (2.1.3):

$$\begin{aligned}\langle \boldsymbol{p}_i m_{s_i}|\hat{\boldsymbol{\alpha}}\boldsymbol{u}_\lambda\, \mathrm{e}^{\mathrm{i}\boldsymbol{kr}}|\boldsymbol{p}_f m_{s_f}\rangle =& 8\sqrt{2}\pi^2 \sum_{\kappa_i\kappa_f}\sum_{\mu_i\mu_f}\sum_{LM}\frac{[L,l]^{\frac{1}{2}}}{[j]^{\frac{1}{2}}}\mathrm{i}^{L+l_f-l_i}\,\mathrm{e}^{-\mathrm{i}(\Delta_{\kappa_i}+\Delta_{\kappa_f})}\\ &\times (l_i 0\tfrac{1}{2}m_{s_i}|j_i\mu_i)(l_f m_{l_f}\tfrac{1}{2}m_{s_f}|j_f\mu_f)(j_f\mu_f LM|j_i\mu_i)\\ &\times D^L_{M\lambda}\mathrm{Y}^*_{l_f m_{l_f}}\sum_p(\mathrm{i}\lambda)^p\langle\varepsilon_i\kappa_i||\hat{\boldsymbol{\alpha}}\boldsymbol{a}^{(p)}_L||\varepsilon_f\kappa_f\rangle\end{aligned} \tag{2.5.1}$$

Here all the parameters belonging to the initial state are indexed with an i, the final state parameters with an f. Also we introduce the symbol $[\cdot]$ as:

$$[j_1, j_2, \ldots, j_n] = (2j_1+1)(2j_2+1)\ldots(2j_n+1) \tag{2.5.2}$$

We now pay attention to the reduced matrix elements $\langle\varepsilon_i\kappa_i||\hat{\boldsymbol{\alpha}}\boldsymbol{a}^{(p)}_L||\varepsilon_f\kappa_f\rangle$. Since we were able to split all our building blocks into an angular and a radial part we should use this opportunity to do the same with the reduced matrix element. Using (2.3.2), (2.4.4) and (2.4.5) one arrives at

$$\begin{aligned}\langle\varepsilon_i\kappa_i||\hat{\boldsymbol{\alpha}}\boldsymbol{a}^{(p)}_L||\varepsilon_f\kappa_f\rangle =& \mathrm{i}\Big(\langle g_{\varepsilon_i\kappa_i}|\mathrm{j}_L|f_{\varepsilon_f\kappa_f}\rangle\langle\varepsilon_i\kappa_i||[\mathrm{Y}_\Lambda\otimes\boldsymbol{\sigma}]_L||\varepsilon_f-\kappa_f\rangle\\ &-\langle f_{\varepsilon_i\kappa_i}|\mathrm{j}_L|g_{\varepsilon_f\kappa_f}\rangle\langle\varepsilon_i-\kappa_i||[\mathrm{Y}_\Lambda\otimes\boldsymbol{\sigma}]_L||\varepsilon_f\kappa_f\rangle\Big)\\ &+\lambda\left(\frac{L+1}{2L+1}\right)^{\frac{1}{2}}\Big(\langle f_{\varepsilon_i\kappa_i}|\mathrm{j}_{L-1}|g_{\varepsilon_f\kappa_f}\rangle\langle\varepsilon_i-\kappa_i||[\mathrm{Y}_\Lambda\otimes\boldsymbol{\sigma}]_{L-1}||\varepsilon_f\kappa_f\rangle\\ &-\langle g_{\varepsilon_i\kappa_i}|\mathrm{j}_{L-1}|f_{\varepsilon_f\kappa_f}\rangle\langle\varepsilon_i\kappa_i||[\mathrm{Y}_\Lambda\otimes\boldsymbol{\sigma}]_{L-1}||\varepsilon_f-\kappa_f\rangle\Big)\\ &+\lambda\left(\frac{L}{2L+1}\right)^{\frac{1}{2}}\Big(\langle f_{\varepsilon_i\kappa_i}|\mathrm{j}_{L+1}|g_{\varepsilon_f\kappa_f}\rangle\langle\varepsilon_i-\kappa_i||[\mathrm{Y}_\Lambda\otimes\boldsymbol{\sigma}]_{L+1}||\varepsilon_f\kappa_f\rangle\\ &-\langle g_{\varepsilon_i\kappa_i}|\mathrm{j}_{L+1}|f_{\varepsilon_f\kappa_f}\rangle\langle\varepsilon_i\kappa_i||[\mathrm{Y}_\Lambda\otimes\boldsymbol{\sigma}]_{L+1}||\varepsilon_f-\kappa_f\rangle\Big)\end{aligned} \tag{2.5.3}$$

where $\boldsymbol{\sigma} = \sigma^i \boldsymbol{e}_i$ is the vector with the Pauli matrices as its components. This reduces the integration to calculate the reduced matrix element from a threefold to one single and one twofold integral. The twofold integral over the azimutal and the polar angle can be solved analytically and is well known. In Ref. [1] we find:

$$\langle \varepsilon_i \pm \kappa_i || [\mathrm{Y}_\Lambda \otimes \boldsymbol{\sigma}]_L || \varepsilon_f \mp \kappa_f \rangle = \sqrt{\frac{3}{2\pi}} (-1)^{l_f} [j_i, j_f, l_i, l_f, L]^{\frac{1}{2}} (l_i 0 l_f 0 | \Lambda 0) \begin{Bmatrix} j_i & l_i & 1/2 \\ j_f & l_f & 1/2 \\ L & \Lambda & 1 \end{Bmatrix} \quad (2.5.4)$$

The radial integrals $\langle g_{\varepsilon_i \kappa_i} | \mathrm{j}_L | f_{\varepsilon_f \kappa_f} \rangle$ and $\langle g_{\varepsilon_i \kappa_i} | \mathrm{j}_L | f_{\varepsilon_f \kappa_f} \rangle$ have to be solved numerically.

2.6 Radial Integrals

As pointed out in the last section the solution of the radial integrals has to be found numerically. One way to do this is discussed in this section.

The radial integrals are:

$$\langle g_{\varepsilon_i \kappa_i} | \mathrm{j}_L | f_{\varepsilon_f \kappa_f} \rangle = \int_0^\infty \mathrm{d}r\, r^2 g_{\varepsilon_i \kappa_i}(r) \mathrm{j}_L(kr) f_{\varepsilon_f \kappa_f}(r) = \int_0^\infty \mathrm{d}r\, I_{gf} \quad (2.6.1a)$$

$$\langle f_{\varepsilon_i \kappa_i} | \mathrm{j}_L | g_{\varepsilon_f \kappa_f} \rangle = \int_0^\infty \mathrm{d}r\, r^2 f_{\varepsilon_i \kappa_i}(r) \mathrm{j}_L(kr) g_{\varepsilon_f \kappa_f}(r) = \int_0^\infty \mathrm{d}r\, I_{fg} \quad (2.6.1b)$$

These integrals cannot be calculated by integrating along the real axis. The integrands are highly oszillating and slowly decreasing for large values of r which is shown in Fig. 2.2. Hence the integration is performed by rotating the integration contour in the complex plane. In order to do this we express the radial functions in terms of Whittaker functions of the first kind $\mathrm{M}_{ab}(z)$:

$$g_{\varepsilon\kappa}(r) = N_\kappa \sqrt{\varepsilon + 1} \left(2pr\right)^{-\frac{3}{2}} \Re \left(\mathrm{e}^{\mathrm{i}(\delta_\kappa - \frac{\pi}{2}(s+\frac{1}{2}))} \left(s + \mathrm{i}\eta\right) \mathrm{M}_{-\frac{1}{2} - \mathrm{i}\eta, s}(2\mathrm{i}pr) \right) \quad (2.6.2a)$$

$$f_{\varepsilon\kappa}(r) = -N_\kappa \sqrt{\varepsilon - 1} \left(2pr\right)^{-\frac{3}{2}} \Im \left(\mathrm{e}^{\mathrm{i}(\delta_\kappa - \frac{\pi}{2}(s+\frac{1}{2}))} \left(s + \mathrm{i}\eta\right) \mathrm{M}_{-\frac{1}{2} - \mathrm{i}\eta, s}(2\mathrm{i}pr) \right) \quad (2.6.2b)$$

We can now express Eq. (2.6.1) in terms of integrals of the form:

$$I_{\alpha_1\gamma_1\alpha_2\gamma_2 L}(p_1, p_2, k) = \int_0^\infty \mathrm{d}r\, r^{-1} \mathrm{M}_{\alpha_1\gamma_1}(2\mathrm{i}p_1 r) \mathrm{M}_{\alpha_2\gamma_2}(2\mathrm{i}p_2 r) \mathrm{j}_L(kr) \quad (2.6.3)$$

If we now express the Whittaker functions of the first kind like

$$\mathrm{M}_{\alpha\gamma}(z) = \frac{\Gamma(2\gamma+1)}{\Gamma(\gamma - \alpha + \frac{1}{2})} \mathrm{e}^{\mathrm{i}\pi s\alpha} \mathrm{W}_{-\alpha\gamma}(-z) + \frac{\Gamma(2\gamma+1)}{\Gamma(\gamma + \alpha + \frac{1}{2})} \mathrm{e}^{\mathrm{i}\pi s(\alpha - \gamma - \frac{1}{2})} \mathrm{W}_{\alpha\gamma}(z) \quad (2.6.4)$$

where $s = 1$ if $\Im(z) < 0$ and $s = -1$ otherwise and $W_{\alpha\gamma}(z)$ are the Whittaker functions of the second kind (see e.g. Ref. [4]). Once this is done the asymptotic behaviour of the Whittaker function shows us that we can split the integral into two parts, one exponentially decreasing in the upper and one exponentially decreasing in the lower half of the complex plane.

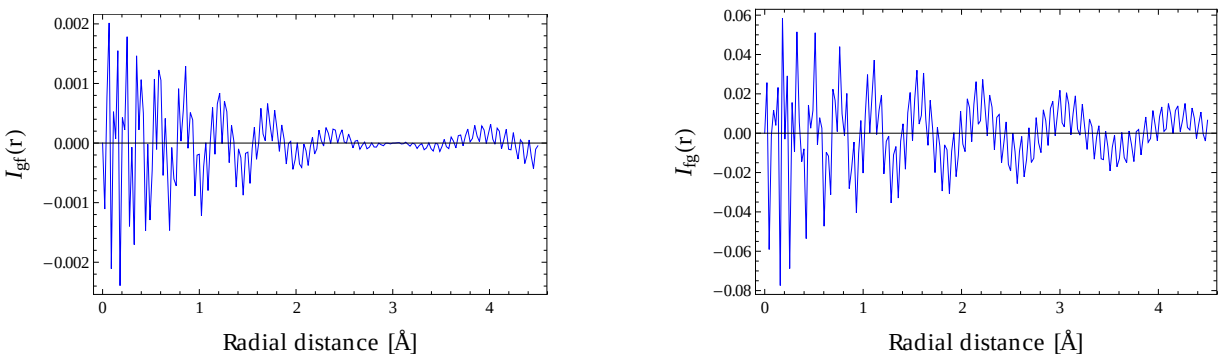

Figure 2.2: Radial integrands $I_{gf}(r)$ (left) and $I_{fg}(r)$ (right) calculated for a nuclear charge of $Z = 79$, $\kappa_i = \kappa_f = 1$, $\varepsilon_i = 1\,\mathrm{keV}$ and $\varepsilon_f = 1\,\mathrm{eV}$.

To evade irregularities for small values of r the integration is performed in two steps. First along the real axis up to a certain value R and for $r > R$ along the rotated integration contour in the complex plane. This method was first described by Vincent and Fortune [5]. An application to the bremsstrahlung process was done by Yerokhin and Surzhykov [6].

3 Density Matrix for ordinary Bremsstrahlung

Once a system is not closed one cannot describe it using a single Hilbert space vector. Instead the *statistical* or *density operator* is used. It describes a mixed state performing a weighted projection $\hat{P}_n$ on a complete basis set $|\psi_n\rangle$ of the Hilbert space:

$$\hat{\varrho} = \sum_n \varrho_n |\psi_n\rangle \langle\psi_n| = \sum_n \varrho_n \hat{P}_n \tag{3.0.1}$$

By choosing a certain representation $|\xi\rangle$ of the eigenstates one gets the density matrix which reads:

$$M_{\xi\xi'} = \langle\xi|\hat{\varrho}|\xi'\rangle \tag{3.0.2}$$

This matrix contains all information about the system. For this reason the statistical operator is often seen as a generalisation of the state vector.

3.1 Application to Bremsstrahlung

To describe the bremsstrahlung process we set our frame to be the rest frame of the atom. The z-axis is set along the asymptotic momentum of the incident electron. The plane defined by $\boldsymbol{p}_i$ and the momentum of the emitted photon $\boldsymbol{k}$ is chosen to be the xz-plane (also called *reaction plane*).

We can get the final state density matrix, the density matrix after the scattering process, from the initial state by a multiplication with the matrix elements (2.5.1). As the scattered electron is not observed we perform an integration over the scattering angle and sum over the spin projection of the scattered electron (see also Sec. 2.3):

$$\begin{aligned}\langle \boldsymbol{k}\lambda|\hat{\varrho}_f|\boldsymbol{k}\lambda'\rangle = \int \mathrm{d}\Omega_f \sum_{m_{s_i} m'_{s_i} m_{s_f}} & \langle \boldsymbol{p_i} m_{s_i}|\hat{\varrho}_i|\boldsymbol{p_i} m'_{s_i}\rangle \\ & \times \langle \boldsymbol{p_i} m_{s_i}|\hat{\boldsymbol{\alpha}}\boldsymbol{u}_\lambda \, \mathrm{e}^{\mathrm{i}\boldsymbol{kr}}|\boldsymbol{p_f} m_{s_f}\rangle^* \langle \boldsymbol{p_i} m'_{s_i}|\hat{\boldsymbol{\alpha}}\boldsymbol{u}_{\lambda'} \, \mathrm{e}^{\mathrm{i}\boldsymbol{kr}}|\boldsymbol{p_f} m_{s_f}\rangle\end{aligned} \tag{3.1.1}$$

Here we chose the representation of the finals state to be $|\boldsymbol{k}\lambda\rangle$ with the photon momentum $\boldsymbol{k}$ and the helicity $\lambda = \pm 1$. The initial state is described by the asymptotic momentum and the spin of the incident electron. As one can find in Ref. [1] the initial state density matrix can be expressed in terms of the statistical tensor $\varrho^{(i)}_{kq}$

$$\langle \boldsymbol{p_i} m_{s_i}|\hat{\varrho}_i|\boldsymbol{p_i} m'_{s_i}\rangle = \sum_{kq} (-1)^{\frac{1}{2}-m'_{s_i}} (\tfrac{1}{2} m_{s_i} \tfrac{1}{2} m'_{s_i}|kq) \varrho^{(i)}_{kq} \tag{3.1.2}$$

where we can express $\varrho^{(i)}_{kq}$ in terms of the components of the polarisation vector of the incoming electron

$$\varrho^{(i)}_{00} = \frac{1}{\sqrt{2}} \qquad \varrho^{(i)}_{10} = \frac{1}{\sqrt{2}} P_z \qquad \varrho^{(i)}_{1\pm1} = \mp\frac{1}{\sqrt{2}}(P_x \mp \mathrm{i}P_y) \tag{3.1.3}$$

where $\boldsymbol{P} = (P_x, P_y, P_z)$ is the polarisation vector of the incoming electron.

Now using the results (2.5.1), (3.1.2), well known symmetry properties and summation relations of Clebsch-Gordan coefficients which could be found e.g. in Ref. [1] one finally obtains:

$$\begin{aligned}\langle \boldsymbol{k}\lambda|\hat{\varrho}_f|\boldsymbol{k}\lambda'\rangle =& 8(2\pi)^4 \sum_{\kappa_i\kappa_i'\kappa_f} \sum_{LL'g} \sum_{krs} (-1)^{2j_i - j_f - j_i' - k + L' + L - l_i} \mathrm{i}^{L'-L+l_i-l_i'} \, \mathrm{e}^{\mathrm{i}(\Delta_{\kappa_i} - \Delta_{\kappa_i'})} \\ & \times \varrho^{(i)}_{k-s} D^r_{st}[j_i, j_i', L, L', l_i, l_i', r, k]^{\frac{1}{2}} (L - \lambda L' \lambda' | r\, t)(l_i 0 l_i' 0 | g 0) \\ & \times (ksr - s | g 0) \begin{Bmatrix} L & j_f & j_i \\ j_i' & r & L' \end{Bmatrix} \begin{Bmatrix} 1/2 & 1/2 & k \\ j_i' & j_i & r \\ l_i' & l_i & g \end{Bmatrix} \\ & \times \sum_{pp'} (-\mathrm{i}\lambda)^p (-\mathrm{i}\lambda')^{p'} \langle \varepsilon_i \kappa_i || \hat{\boldsymbol{\alpha}} \boldsymbol{a}^{(p)}_L || \varepsilon_f \kappa_f \rangle^* \langle \varepsilon_i \kappa_i' || \hat{\boldsymbol{\alpha}} \boldsymbol{a}^{(p')}_{L'} || \varepsilon_f \kappa_f \rangle \end{aligned} \tag{3.1.4}$$

The number of summands in this formula is mainly determined by the number of partial waves needed for the reduced matrix elements to converge up to a certain precision. All other summation limits cannot be chosen arbitrary because the Clebsch-Gordan coefficients vanish if the triangle conditions are not satisfied. The only exceptions are k and s. In the general case they are always $k \in \{0, 1\}$ and $-k \leq s \leq k$.

3.2 Convergence

The main influence on the convergence behaviour of the reduced matrix element is the energy of the electrons (incident and scattered). The partial waves expansion converges very fast for low electron energies. For higher energies the convergence slows down and more partial waves are needed to achieve the desired precision.

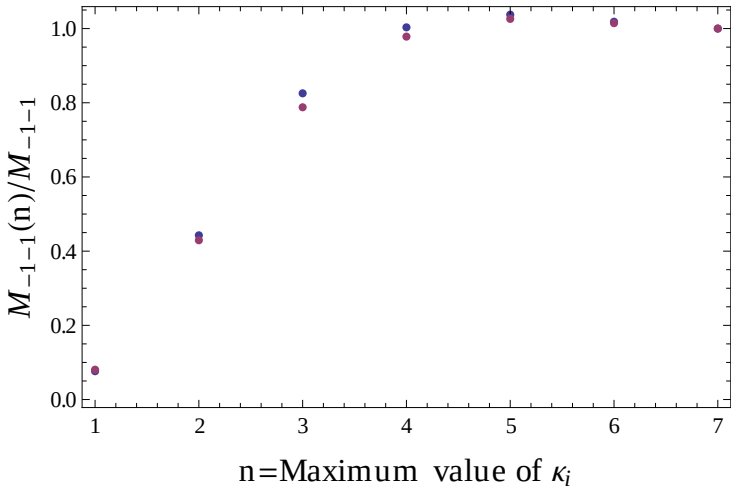

Figure 3.1: Normalised density matrix element $\lambda = \lambda' = -1$ for different energies (blue: $\varepsilon_i = 100\,\text{keV}$, red: $\varepsilon_i = 80\,\text{keV}$) and $\varepsilon_f = 1\,\text{eV}$ always while the observation angle is fixed to 60°.

Fig. 3.1 shows us the convergence behaviour of the M_{-1-1} density matrix element for 100 keV and 80 keV in comparison with a fixed observation angle. Therefor the absolut values of M_{-1-1} were normalised to the converging point in both cases. In this example only the expansion of the initial electron was taken into account while the energy of the scattered electron is fixed and summation is perfomed till convergence. It is apparent that the density matrix element converges slower in the 100 keV case. The finding of this is that all calculations are more time expensive for higher energies.

4 Observables of Atomic Bremsstrahlung

There are two properties of bremsstrahlung mainly observed in experiments. The angular distribution and especially asymmetries of radiation intensity within the reaction plane are characteristics which can easily be measured. Additionally modern experimental techniques give us access to polarisation properties of the bremsstrahlung radiation.

4.1 Angular distribution

In this section we will derive an expression for the cross section differential in the observation angle and the photon energy. This allows us to investigate the angular properties of bremsstrahlung radiation.

For all further derivations we normalise the trace of $\hat{\varrho}$ related to the cross section following Tseng and Pratt [7] and Yerokhin and Surzhykov [6] as

$$\sigma(k) = \frac{k}{Z^2}\frac{\mathrm{d}\sigma}{\mathrm{d}k} = 2\pi\int_{-1}^{1}\mathrm{d}(\cos\vartheta_k)\frac{\mathrm{d}\sigma}{\mathrm{d}k\,\mathrm{d}\Omega_k} = \frac{1}{32\pi}\frac{k^2}{p_i^2}\frac{\alpha}{Z^2}\int_{-1}^{1}\mathrm{d}(\cos\vartheta_k)\mathrm{Tr}(\hat{\varrho}) \tag{4.1.1}$$

where k is the energy of the emitted photon, p_i the absolute value of the initial electron momentum and Ω_k the solid angle of the emitted photon. The angle ϑ_k denotes the angle between $\boldsymbol{p}_i$ and $\boldsymbol{k}$ in the xz-plane.

This directly leads us to the double differential cross-section:

$$\frac{\mathrm{d}\sigma}{\mathrm{d}k\,\mathrm{d}\Omega_k} = \frac{\alpha}{64\pi^2}\frac{k^2}{Z^2 p_i^2}\mathrm{Tr}(\hat{\varrho}_f) \tag{4.1.2}$$

4.1.1 Parametrisation of the Double Differential Cross-Section

In order to find a more convenient expression we make use of (3.1.4) and (2.1.2c). This allows us to express the trace of the density matrix as a weighted sum of spherical harmonics

$$\mathrm{Tr}(\hat{\varrho}_f) = 256\pi^{\frac{9}{2}}\sum_{rs}\mathrm{C}_{rs}^{(A)}\mathrm{Y}_{r,-s} \tag{4.1.3}$$

where the angular coefficients $\mathrm{C}_{rs}^{(A)}$ are defined by:

$$\begin{aligned}\mathrm{C}_{rs}^{(A)} = &\sum_{\kappa_i\kappa_i'\kappa_f}\sum_{LL'g}\sum_{kpp'}(-1)^{2j_i-2j_f-j_i'-k+L+L'-l_i+s}\left((-1)^p+(-1)^{p'+L+L'-r}\right)\mathrm{i}^{L'-L+l_i-l_i'+p+p'}\\ &\times \mathrm{e}^{\mathrm{i}(\Delta_{\kappa_i}-\Delta_{\kappa_i'})}\varrho_{k,-s}^{(i)}[j_i,j_i',L,L',l_i,l_i',k]^{\frac{1}{2}}(l_i0l_i'0|g0)(ksr-s|g0)(L-1L'1|r0)\\ &\times\begin{Bmatrix}L & j_f & j_i\\ j_i' & r & L'\end{Bmatrix}\begin{Bmatrix}{}^1/_2 & {}^1/_2 & k\\ j_i' & j_i & r\\ l_i' & l_i & g\end{Bmatrix}\langle\varepsilon_i\kappa_i||\hat{\boldsymbol{\alpha}}\boldsymbol{a}_L^{(p)}||\varepsilon_f\kappa_f\rangle\langle\varepsilon_i\kappa_i'||\hat{\boldsymbol{\alpha}}\boldsymbol{a}_{L'}^{(p')}||\varepsilon_f\kappa_f\rangle\end{aligned}\tag{4.1.4}$$

Inserting this result into Eq. (4.1.2) we get the following expression for the double differential cross section:

$$\frac{\mathrm{d}\sigma}{\mathrm{d}k\,\mathrm{d}\Omega_k} = 4\pi^{\frac{5}{2}}\frac{\alpha k^2}{Z^2p_i^2}\sum_{rs}\mathrm{C}_{rs}^{(A)}\mathrm{Y}_{r,-s}\tag{4.1.5}$$

As pointed out before (see 3.1) the summation index r is determined by the maximum value of κ_i ($n_i = \max(\kappa_i)$ while s can only take the values 0 or ±1. The triangle conditions for the Wigner-6j symbol [1] lead us to the following equation for the number of coefficients N_A in the most general case:

$$N_A = 3(2n_i-1)\tag{4.1.6}$$

This can be reduced using further properties of the $\mathrm{C}_{rs}^{(A)}$ which will be discussed in the next section 4.1.2.

4.1.2 Properties of the Angular Coefficients

One influent factor we have not taken into account yet is the polarisation of the incident electron respectively its counterpart in the equation $\varrho_{k,-s}^{(i)}$ (see Eq. (3.1.3)). There are four different possibilities for the electron polarisation. It can be unpolarised, polarised transversely within and perpendicularly to the reaction plane and longitudinally polarised. The symmetry properties of $\varrho_{k,-s}^{(i)}$ and the angular coefficients in Eq. (3.1.4) now show us that the density matrix elements stay same no matter if the electron is polarised transversly in x- or longitudinally in z-direction (see Ref. [6]). The spherical harmonics do not fulfill a symmetry relation in the second index which would allow to cancel the contribution of the summands with $s \neq 0$. That means only the coefficients $\mathrm{C}_{r0}^{(A)}$ are nonzero which reduces the number of coefficients by the factor of one third. In case of an electron polarised perpendicularly to the xz-plane one obtains the symmetry relation:

$$\mathrm{C}_{r,-s}^{(A)} = -\mathrm{C}_{rs}^{(A)}\tag{4.1.7}$$

This reduces the number of coefficients at least to two thirds of the number mentioned in Eq. (4.1.6). The final results of these considerations according to number of coefficients needed for the calculation are shown in Tab. 4.1.

Another useful property is that the angular coefficients with $s = 0$ do not change when the polarisation of the electron changes. That means in the case of different polarisations it is not necessary to calculate the $\mathrm{C}_{r0}^{(A)}$ factors again. Just the $\mathrm{C}_{r1}^{(A)}$-coefficients change and have to be calculated in addition.

Table 4.1: Number of independent $C_{rs}^{(A)}$-coefficients for different initial electron polarisations and a certain n_i. Also the main symmetry of the coefficients is pointed out.

Polarisation	P_x	P_y	P_z	N_A	Symmetry
unpolarised	0	0	0	$2n_i-1$	only $\varrho_{00}^{(i)} \neq 0$
transversely	1	0	0	$2n_i-1$	same density matrix as $\boldsymbol{P}=0_v$
longitudinally	0	0	1	$2n_i-1$	same density matrix as $\boldsymbol{P}=0_v$
perpendicularly	0	1	0	$2(2n_i-1)$	$C_{rs}^{(A)}$ odd in s

4.2 Stokes Parameters and Degree of Linear Polarisation

To describe polarisation phenomena it is convenient to use the *Stokes parameters* P_1, P_2 and P_3. P_1 and P_2 describe the linear polarisation of a photon, while P_3 carries the degree of cirular polarisation. The parameters P_1 and P_2 are facile available to measurements by recording the intensity of the emitted light with a certain polarisation angle with respect to the reaction plane:

$$P_1 = \frac{I_{0^\circ} - I_{90^\circ}}{I_{0^\circ} + I_{90^\circ}} \qquad P_2 = \frac{I_{45^\circ} - I_{135^\circ}}{I_{45^\circ} + I_{135^\circ}} \tag{4.2.1}$$

Often also the degree of linear polarisation P_L is measured. Therefor the coordinate system is chosen to be elliptic. This leads us to

$$P_L = \sqrt{P_1^2 + P_2^2} \qquad \chi = \frac{1}{2}\arctan\frac{P_2}{P_1} \tag{4.2.2}$$

with the polarisation angle χ.

The final state density matrix of the atomic system also contains all information about the polarisation of the emitted photon as described in Ref. [1]:

$$\langle \boldsymbol{k}\lambda|\hat{\varrho}_f|\boldsymbol{k}\lambda'\rangle = \frac{1}{2}\mathrm{Tr}(\hat{\varrho}_f)\begin{pmatrix} 1+P_3 & P_1 - \mathrm{i}P_2 \\ P_1 + \mathrm{i}P_2 & 1-P_3 \end{pmatrix} \tag{4.2.3}$$

From this equation we can get the degree of linear polarisation. It is evident that P_L does not include squared terms. Only the mixed terms of the secondary diagonal density matrix elements is kept:

$$P_L = \frac{2}{\mathrm{Tr}(\hat{\varrho}_f)}\left(\langle \boldsymbol{k}1|\hat{\varrho}_f|\boldsymbol{k}-1\rangle\,\langle \boldsymbol{k}-1|\hat{\varrho}_f|\boldsymbol{k}1\rangle\right)^{\frac{1}{2}} \tag{4.2.4}$$

4.2.1 Parametrisation of the Degree of Linear Polarisation

Using again Eq. (3.1.4) we find a very similar parametrisation to Eq. (4.1.3):

$$P_L = \frac{\sqrt{2}}{\pi^{\frac{1}{4}}}\left(\sum_{rs} C_{rs}^{(A)} Y_{r,-s}\right)^{-1}\left(\sum_{b\beta} C_{b\beta}^{(P)} Y_{b,-\beta}\right)^{\frac{1}{2}} \tag{4.2.5}$$

Table 4.2: Number of independent $\mathrm{C}_{b\beta}^{(P)}$ coefficients for different initial electron polarisations and a certain n_i. Also the main symmetry is pointed out.

Polarisation	P_x	P_y	P_z	N_P	Symmetry
unpolarised	0	0	0	$2(2n_i-1)$	only $\varrho_{00}^{(i)} \neq 0$
transversely	1	0	0	$6(2n_i-1)$	$\mathrm{C}_{b\beta}^{(P)}$ even in β
longitudinally	0	0	1	$2(2n_i-1)$	only $\mathrm{C}_{b0}^{(P)} \neq 0$ because $s=0$
perpendicularly	0	1	0	$6(2n_i-1)$	$\mathrm{C}_{b\beta}^{(P)}$ even/odd in $\lvert\beta\rvert = 1,2$

Here we introduced the $\mathrm{C}_{b\beta}^{(P)}$-coefficients describing the polarisation properties of the bremsstrahlung radiation while also the $\mathrm{C}_{rs}^{(A)}$ coefficients are included to calculate the trace of $\hat{\varrho}_f$. In order to make the expression for the $\mathrm{C}_{b\beta}^{(P)}$-coefficients more convenient to read we introduce the following symbol which generates the expression between the previous two delimiters again with tilded indices:

$$\big(f(a_1,a_2,\ldots,a_n)\big)\cdot\widetilde{\big(\bullet\big)} = f(a_1,a_2,\ldots,a_n)\cdot f(\tilde{a}_1,\tilde{a}_2,\ldots,\tilde{a}_n) \tag{4.2.6}$$

Now the coefficients read:

$$\begin{aligned}
\mathrm{C}_{b\beta}^{(P)} = \sum_{\kappa_i\kappa_i'\kappa_f}\sum_{LL'g}\sum_{krs}\sum_{pp'}\sum_{\widetilde{(\bullet)}}\Big((-1)^{2j_i-j_f-j_i'-k+L'+L-l_i}\mathrm{i}^{L'-L+l_i-l_i'+p+p'}\,\mathrm{e}^{\mathrm{i}(\Delta_{\kappa_i}-\Delta_{\kappa_i'})}\varrho_{k,-s}^{(i)}\\
\times[j_i,j_i',L,L',l_i,l_i',r,k]^{\frac{1}{2}}(l_i0l_i'|g0)(ksr-s|g0)\begin{Bmatrix} L & j_f & j_i \\ j_i' & r & L'\end{Bmatrix}\begin{Bmatrix} {}^1/_2 & {}^1/_2 & k \\ j_i' & j_i & r \\ l_i' & l_i & g\end{Bmatrix}\\
\times\langle\varepsilon_i\kappa_i||\hat{\boldsymbol{\alpha}}\boldsymbol{a}_L^{(p)}||\varepsilon_f\kappa_f\rangle\langle\varepsilon_i\kappa_i'||\hat{\boldsymbol{\alpha}}\boldsymbol{a}_{L'}^{(p')}||\varepsilon_f\kappa_f\rangle\Big)\widetilde{\big(\bullet\big)}\sum_{b\beta}(-1)^{p+p'+\beta}[b]^{-\frac{1}{2}}(L1L'1|r2)\\
\times(\tilde{L}-1\tilde{L}'-1|\tilde{r}-2)(rs\tilde{r}\tilde{s}|b\beta)(r2\tilde{r}-2|b0)
\end{aligned} \tag{4.2.7}$$

With a look at the triangle conditions one obtains the corresponding number of $\mathrm{C}_{b\beta}^{(P)}$ coefficients to a certain n_i to be

$$N_P = 10(2n_i-1) \tag{4.2.8}$$

This number can also be denotatively reduced.

4.2.2 Properties of the Polarisation Coefficients

It is obvious that more coefficients are needed for the calculation of the polarisation properties. Taking again the electron polarisation into account we find three cases in which the number of coefficients is reduced due to symmetry relations shown in Tab. 4.2.

The symmetry relation for longitudinally polarised electrons can be seen in the Clebsch-Gordan coefficient $(rs\tilde{r}\tilde{s}|b\beta)$ in Eq. (4.2.7). The statistical tensor (3.1.3) vanishes for $s\neq 0$ but if $s=0$ the Clebsch-Gordan coefficient vanishes if $\beta\neq 0$, so only the coefficients $\mathrm{C}_{b0}^{(P)}$ are nonzero. For transversely and perpendicularly polarised electrons it can be found that $\mathrm{C}_{b,-1}^{(P)} = \pm\mathrm{C}_{b1}^{(P)}$

and $C^{(P)}_{b,-2} = C^{(P)}_{b2}$ where the upper sign describes transversly and the lower perpendicularly polarised electrons.

Similar to the angular coefficients the polarsation ones do not change with every change of the electron polarisation. For the polarisation vectors $\boldsymbol{P} = (0,1,0)$ and $\boldsymbol{P} = (1,0,0)$ the coefficients stay same for $\beta = 0$ and equal each other up to a sign change for $\beta = 2$. But in contrast to the angular coefficients there are no symmetries between the cases of polarised and unpolarised incoming electrons.

5 Results and Discussion

In this section the results for the angular distribution as well as the polarisation properties of bremsstrahlung radiation will be discussed. Also the sensitivity of the observables to the electron polarisation and their energy will be treated. However the main part will be the analysis of the behaviour of the expansion coefficients (4.1.4) and (4.2.7).

5.1 Angular distribution

The angular distribution stays same either if the incident electron is unpolarised or polarised within the xz-plane (see 4.1.2). So we restrict ourselves to the two cases where the electron is polarised along the y-axis or not. A comparison between these two cases for different electron energies can be seen in Fig. 5.1. The cross-section decreases for higher electron energies and the maxima are shifted towards the forward scattering region. As one can see the symmetry of the cross-section is sensitive to an electron polarised perpendicularly to the reaction plane. This asymmetry increases with lower photon energies and amounts e.g. for a photon energy of 100 keV to about 7% (discrepancy between the two maxima).

5.2 Angular Coefficients

The behaviour of the angular coefficients is very important in order to decide how many coefficients to take into account. Furthermore to get access to all bremsstrahlung properties for arbitrary initial conditions especially the behaviour of the coefficients for different energies and nuclear charges is important. Fig. 5.2 shows us how the angular coefficients behave for

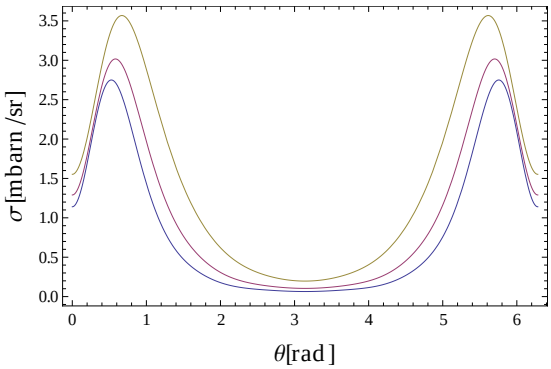

(a) Angular distribution with $\boldsymbol{P} = (0,0,0)$

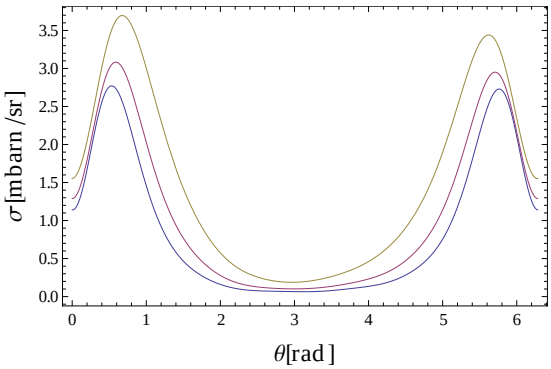

(b) Angular distribution with $\boldsymbol{P} = (0,1,0)$

Figure 5.1: Angular distribution for different polarisations and photon energies ε_i (blue: 200 keV, red: 150 keV, yellow: 100 keV) where $\varepsilon_f = 1$ eV and $Z = 79$ always.

different r. It can be seen that the absolut value of the coefficients decreases rapidly. For a photon energy of 100 keV, $s = 0$ and $r = 10$ it is less than 0.1% of the first value. When $|s| = 1$ it decreases slightly slower and reaches 0.1% of the first value when $r = 11$. In absolute values the coefficients with $|s| = 1$ are about one order of magnitude smaller than the ones with $s = 0$, so the slower decreasing behaviour has less relevance. The detail view in Fig. 5.2c and 5.2d reveales that the convergence is still faster for lower energies.

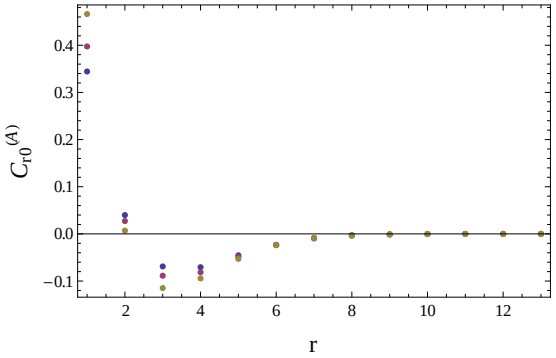

(a) Angular coefficients with $s = 0$

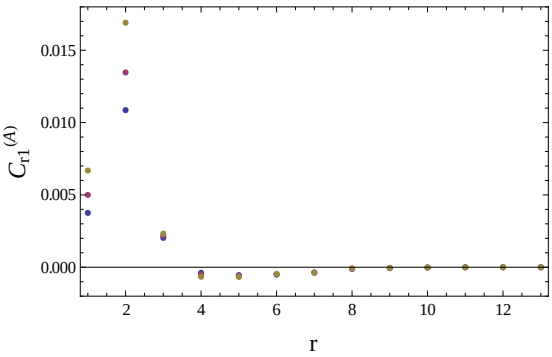

(b) Angular coefficients with $|s| = 1$

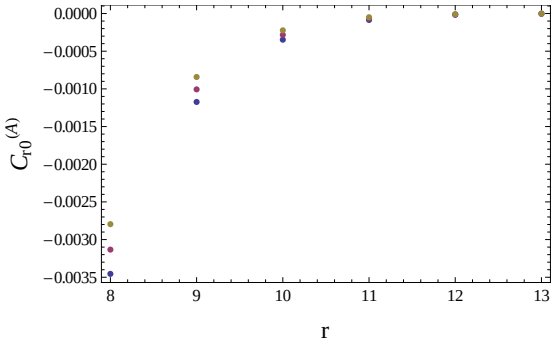

(c) Angular coefficients with $s = 0$ (detail)

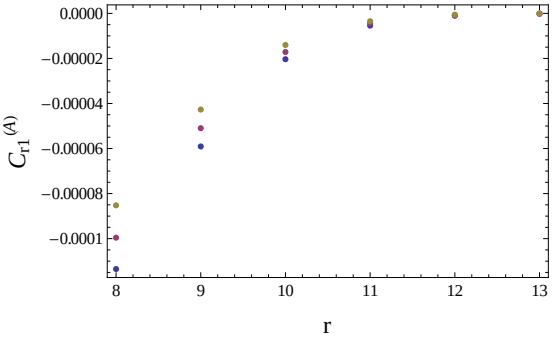

(d) Angular coefficients with $|s| = 1$ (detail)

Figure 5.2: Dependency of the angular coefficients on the summation index r for different energies ε_i (blue: 100 keV, red: 90 keV, yellow: 80 keV) where $\varepsilon_f = 1$ eV and $Z = 79$ always.

Though the expansion was derived from the former work of Yerokhin and Surzhykov it perfectly reproduces the results published by Yerokhin and Surzhykov [6]. In Fig. 5.3 we see that we have very good agreement with the full calculations even with only seven coefficients taken into account. In the backscattering and forward scattering region the calculation is more inaccurate while the relative error is less than 5% for a wide angular range. For the results from the expansion to the ninth order the relative error never exceeds 2%. This is a very promising fact because we can reproduce the results from exact calculations with a very good accuracy with less than ten coefficients.

The coefficients are discrete in the energy because the reduced matrix elements have to be calculated for specific energies. Nevertheless we want to calculate the bremsstrahlung properties for arbitrary energies. In order to achieve this Fig. 5.4 tells that the coefficients behave smooth enough that an interpolation is possible. It also shows that the difference between the coefficients decreases with increasing energies so we can make the grid less narrow for higher energies.

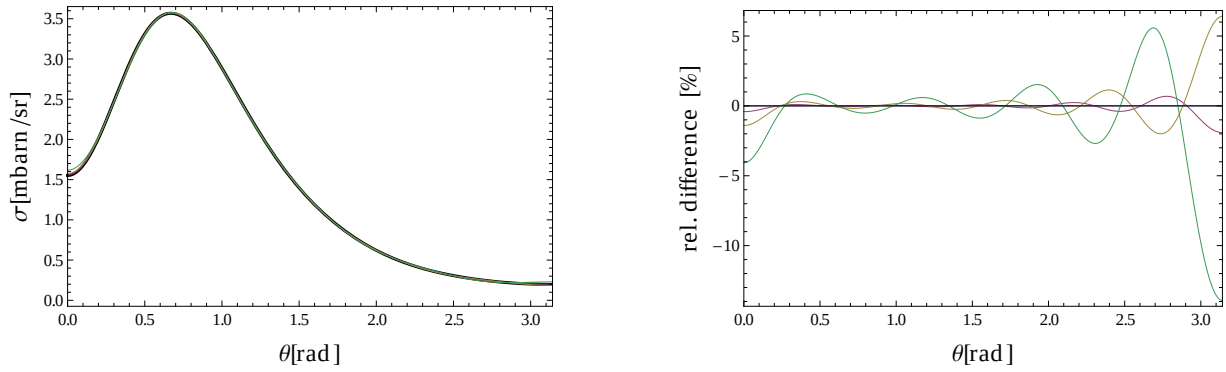

Figure 5.3: Angular distribution and relative error for different orders of the expansion in comparison to the results of Yerokhin and Surzhykov [6] (black) with $r_{max} = 9$ (red), $r_{max} = 8$ (yellow), $r_{max} = 7$ (green), $Z = 79$, $\varepsilon_i = 100\,\text{keV}$, $\varepsilon_f = 1\,\text{eV}$ and unpolarised incident electrons.

Souch an interpolation is done and shown in Fig. 5.7 for an energy of 90 keV for the initial electron and the emitted photon. The interpolating function was chosen lineary. Fig. 5.7 also confirms us that a grid interval of 20 keV is still enough to get results with an error less than 5% compared to the exact calculations. Thus it is possible to calculate the angular distribution respectively the trace of the density matrix for continuus energies.

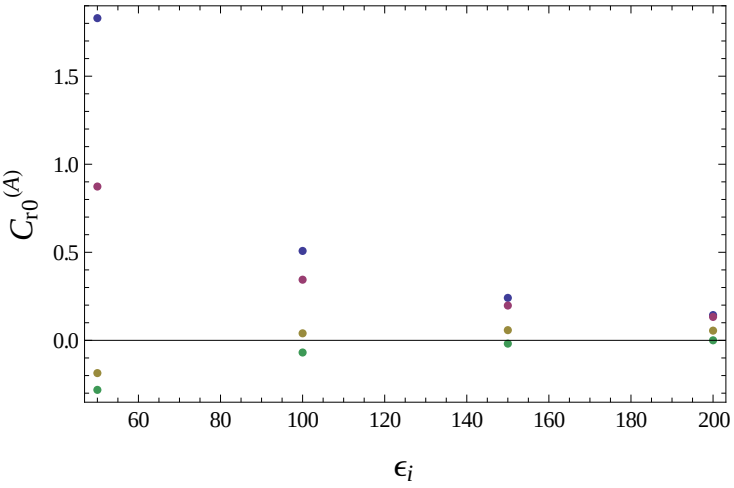

Figure 5.4: Energy dependence of the first four (blue: r=0, red: r=1, yellow: r=2, green: r=3) angular coefficients with $s = 0$, $Z = 79$ and $\varepsilon_f = 1\,\text{eV}$

The second parameter we can vary is the nuclear charge. As Fig. 5.6 shows it is also not necessary to calculate the coefficients for every element. The coefficients change even slower with Z than they do when the enegery is varied. An interpolation example is shown in Fig. 5.5. We achieve a still very good precision (less than 5%) when only every tenth element is calculated while we can get the results for the other elements from a linear interpolation. For higher nuclear charges the coefficients vary slightly faster so the grid should be chosen narrower for higher Z.

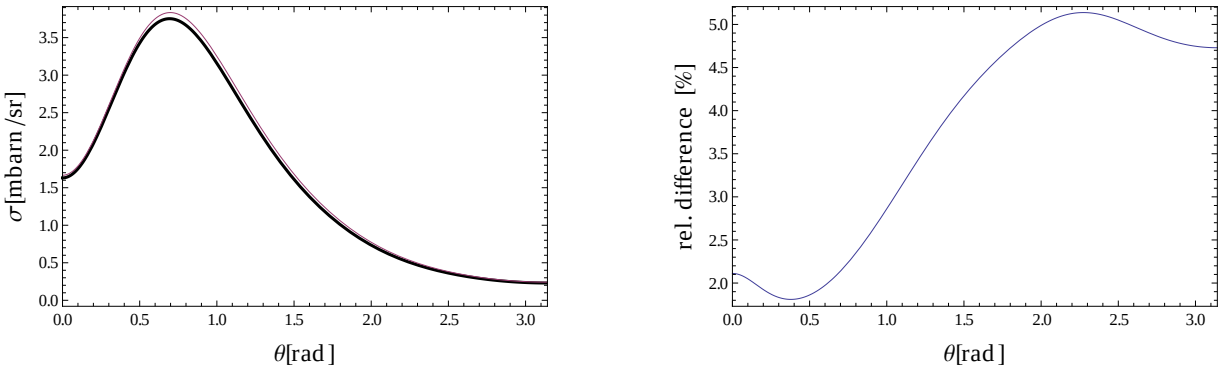

Figure 5.5: Angular distribution calculated with interpolated angular coefficients (red) and relative error (blue, right) in comparison to the exact calculations (black) for $\varepsilon_i =$ 90 keV and $Z = 79$. The interpolation was done lineary between $\varepsilon_i = 80$ keV and $\varepsilon_i = 100$ keV.

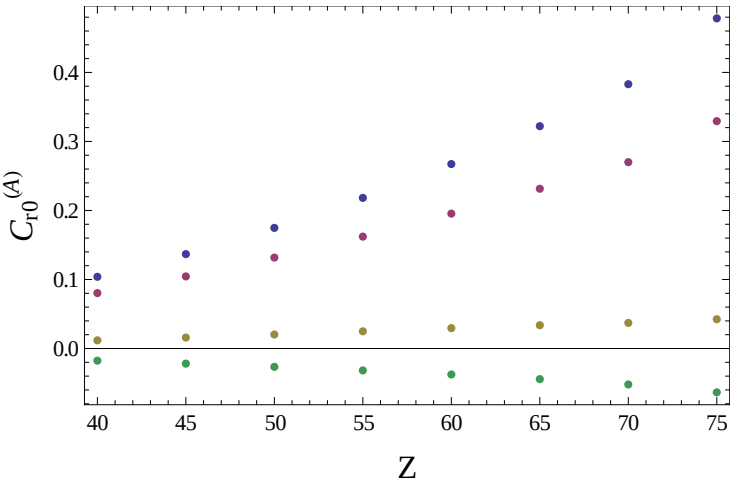

Figure 5.6: Z dependence of the first four (blue: $r = 0$, red: $r = 1$, yellow: $r = 2$, green: $r = 3$) angular coefficients with $s = 0$, $\varepsilon_i = 100$ keV and $\varepsilon_f = 1$ eV

With that knowledge we can tabulate the coefficients to include them in programs or even in analytical calculations. An example how souch a table might look is given in Tab. 5.2.

5.3 Degree of Linear Polarisation

If one considers the degree of linear polarisation one has to discern three cases regarding the polarisation of the incident electron. It stays same for an unpolarised or polarised electron if $\boldsymbol{P} = (0,0,1)$. As shown in Fig. 5.8 it changes remarkably when the incident electron is polarised along the y-axis. For the electron being polarised in the x-direction the graph becomes non differentiable in the symmetry axis. Furthermore the degree of linear polarisation is not very sensitive to the energy of the emitted photon. Only in the case of $\boldsymbol{P} = (0,1,0)$ the value and localisation of the local maximum around π changes.

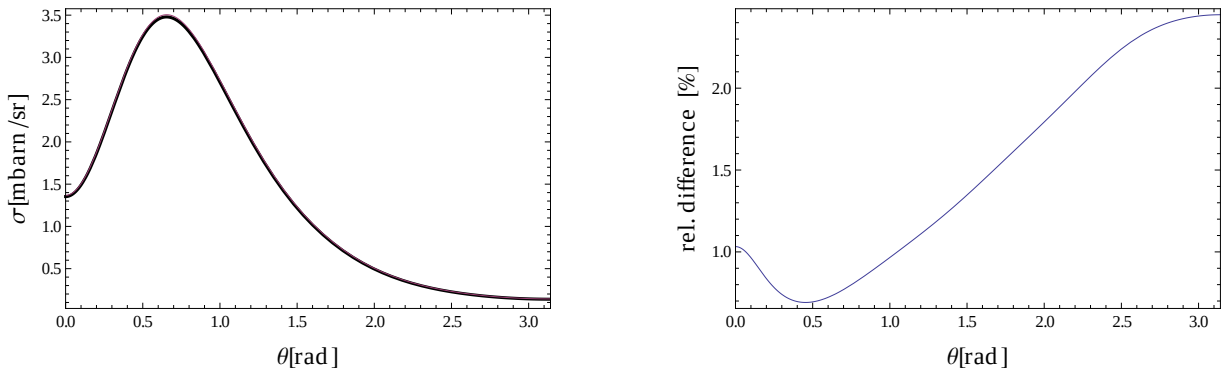

Figure 5.7: Angular distribution calculated with interpolated angular coefficients (red) and relative error (blue, right) in comparison to the exact calculations (black) for $Z = 60$ and $\varepsilon_i = 100\,\text{keV}$. The interpolation was done lineary between $Z = 55$ and $Z = 65$.

Table 5.1: Example table for the angular coefficients with $\varepsilon_i = 100\,\text{keV}$, $\varepsilon_f = 1\,\text{eV}$, $Z = 79$ and $\boldsymbol{P} = (0,1,0)$

r	s	$C_{rs}^{(A)}$	r	s	$C_{rs}^{(A)}$
0	0	0.507724302002963	7	0	−0.00947795293744706
0	1	0	7	1	−0.000363319590388501
1	0	0.344398501936081	8	0	−0.0034552983855032
1	1	0.00375785864104833	8	1	−0.000113492766815833
2	0	0.0398815490245401	9	0	−0.00117350981920064
2	1	0.0108615859536079	9	1	$-5.90791861920147 \times 10^{-5}$
3	0	−0.0690212194897701	10	0	−0.000347139388737766
3	1	0.00203077709708729	10	1	$-2.03471645012551 \times 10^{-5}$
4	0	−0.0706543567085907	11	0	$-8.52271316334904e \times 10^{-5}$
4	1	−0.000386051548485655	11	1	$-5.43700045696847 \times 10^{-6}$
5	0	−0.0454458251636845	12	0	$-1.66110811896278 \times 10^{-5}$
5	1	−0.000546896145553714	12	1	$-1.03745657519108e \times 10^{-6}$
6	0	−0.0232652024012356	13	0	$-2.65429283516658e \times 10^{-6}$
6	1	−0.000504003977197155	13	1	$-1.73033238817568e \times 10^{-7}$

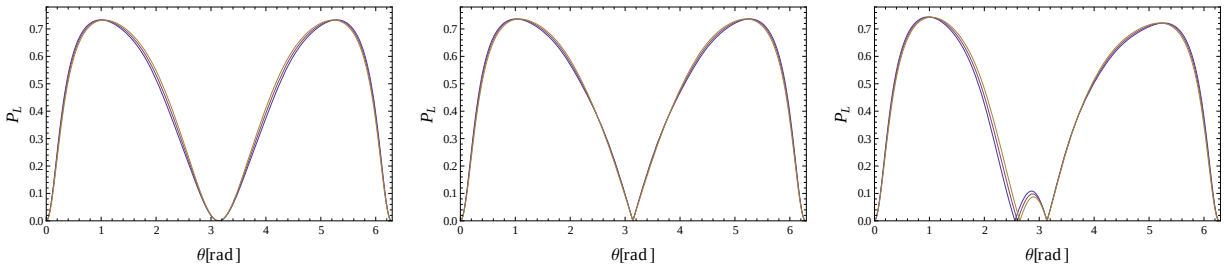

(a) $\boldsymbol{P} = (0,0,0)$ or $\boldsymbol{P} = (0,0,1)$ (b) $\boldsymbol{P} = (1,0,0)$ (c) $\boldsymbol{P} = (0,1,0)$

Figure 5.8: Degree of linear polarisation for different electron polarisations and photon energies ε_i (blue: 100 keV, red: 90 keV, yellow: 80 keV) where $\varepsilon_f = 1\,\text{eV}$ and $Z = 79$ always.

5.4 Polarisation Coefficients

Again we want to investigate the convergence behaviour of the expansion coefficients. In Fig. 5.9 it can be seen that the polarisation coefficients converge still quite fast but slower than the angular ones.

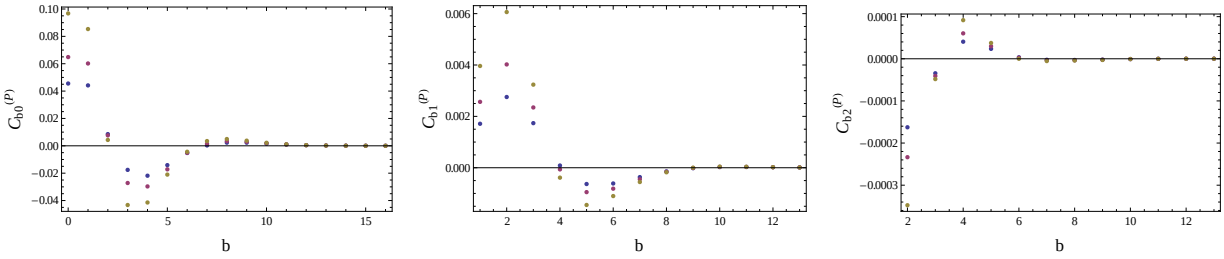

(a) Polarisation coefficients with $\beta = 0$

(b) Polarisation coefficients with $\beta = 1$

(c) Polarisation coefficients with $\beta = 2$

Figure 5.9: Dependency of the polarisation coefficients on the summation index b for different energies ε_i (blue: 100 keV, red: 90 keV, yellow: 80 keV) where $\varepsilon_f = 1$ eV, $Z = 79$ and $\boldsymbol{P} = (0,1,0)$ always.

Since the squareroot is taken of the polarisation expansion the degree of linear polarisation is more sensitive to small changes of the polarisation coefficients. If the expansion is finished too early complex values of P_L might appear.

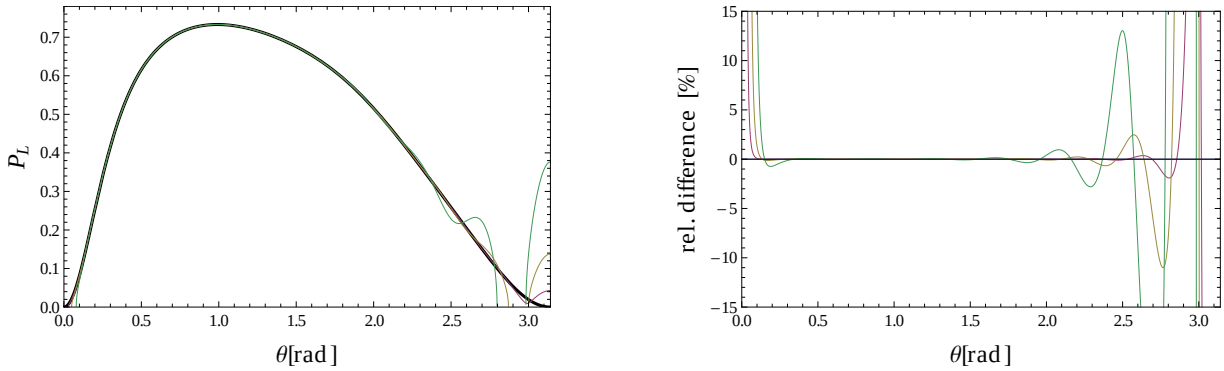

Figure 5.10: Degree of linear polarisation and relative error for different orders of the expansion in comparison to the results of Yerokhin and Surzhykov [6] (black) with $b_{max} = 18$ (red), $b_{max} = 16$ (yellow), $b_{max} = 14$ (green), $Z = 79$, $\varepsilon_i = 100$ keV, $\varepsilon_f = 1$ eV and unpolarised incident electrons. The Trace of $\hat{\varrho}_f$ was calculated following Ref. [6]

From Sec. 4.2.2 we expect that twice the number of coefficients is needed for the polarisation parametrisation in the case of unpolarised incident electrons. Fig. 5.10 illustrates the degree of linear polarisation for different maximum values of b. Although complex values appear in the backscattering area we still reproduce the results of Yerokhin and Surzhykov [6] with an excellent accuracy for angles between 0.2 and 2.2. The intervals where P_L becomes almost zero the difference increases immediately although the absolute error is still small.

As well as the $C_{rs}^{(A)}$-coefficients the polarisation coefficients can be interpolated because they behave similary smooth as shown in Fig. 5.11.

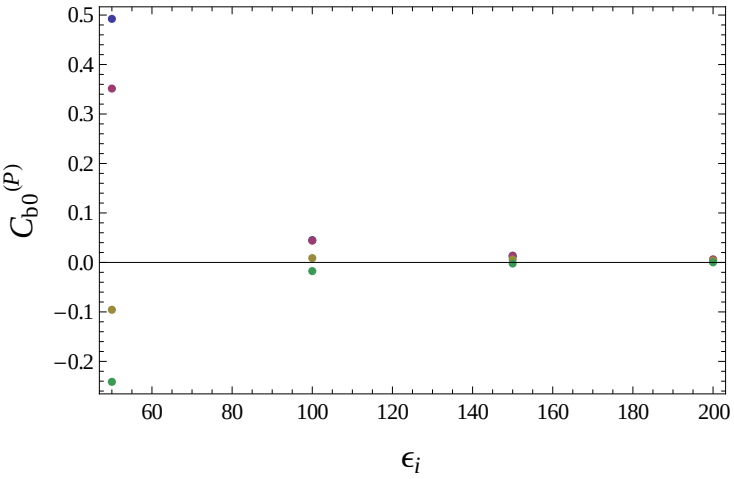

Figure 5.11: Energy dependence of the first four (blue: b=0, red: b=1, yellow: b=2, green: b=3) polarisation coefficients with $\beta = 0$, $Z = 79$, and an unpolarised incident electron.

If we try to interpolate the coefficients for an energy between two nodes we recognise that the degree of linear polarisation is more sensitive to small aberrations of the coefficients. Because of that we choose the distance between the nodes to be 10 keV. The results of these calculations are shown in Fig. 5.12. Again we have very good agreement with the exact results.

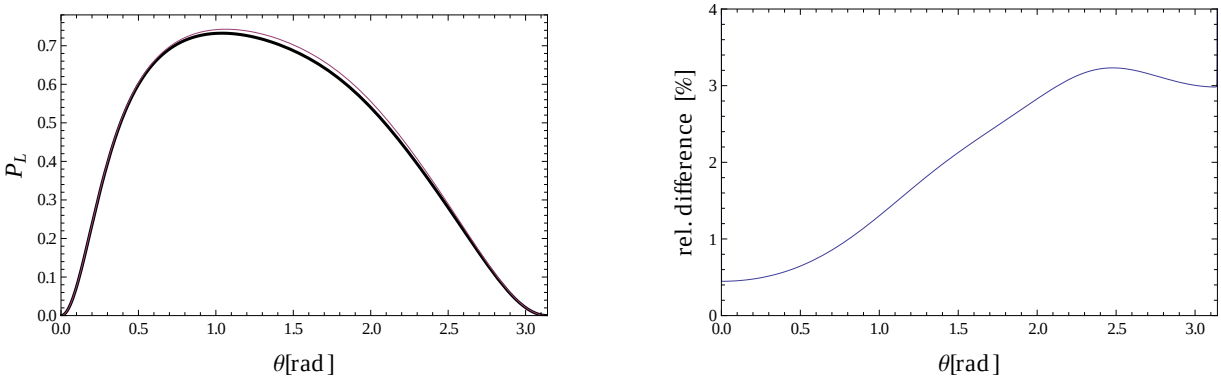

Figure 5.12: Degree of linear polarisation calculated with interpolated polarisation coefficients (red) and relative aberration (blue, right) in comparison to the exact calculations (black) for $\varepsilon_i = 85$ keV and $Z = 79$. The interpolation was done lineary between $\varepsilon_i = 80$ keV and $\varepsilon_i = 90$ keV. For the denomiator of P_L 4.2.4 the exact calculations were used.

The interpolation was done for an energy of 85 keV. To select only the influence of the interpolation of the polarisation coefficients the trace of $\hat{\varrho}_f$ was calculated following Ref. [6].

The polarisation coefficients can also be easily interpolated on the Z-scale as Fig. 5.13 suggests. One should notice that the polarisation coefficients do not need a narrower grid for interpolation than the angular coefficients but still vary faster with increasing nuclear charge. This should be taken into account when the distance between the nodes is set. As expected we achieve again a very good agreement with the exact calculations what can be seen in Fig. 5.14.

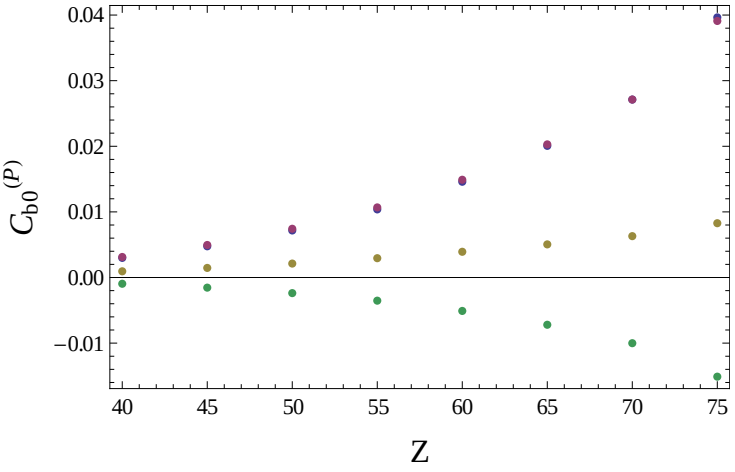

Figure 5.13: Z dependence of the first four (blue: r=0, red: r=1, yellow: r=2, green: r=3) polarisation coefficients with $\beta = 0$, $\varepsilon_i = 100\,\text{keV}$ and $\varepsilon_f = 1\,\text{eV}$

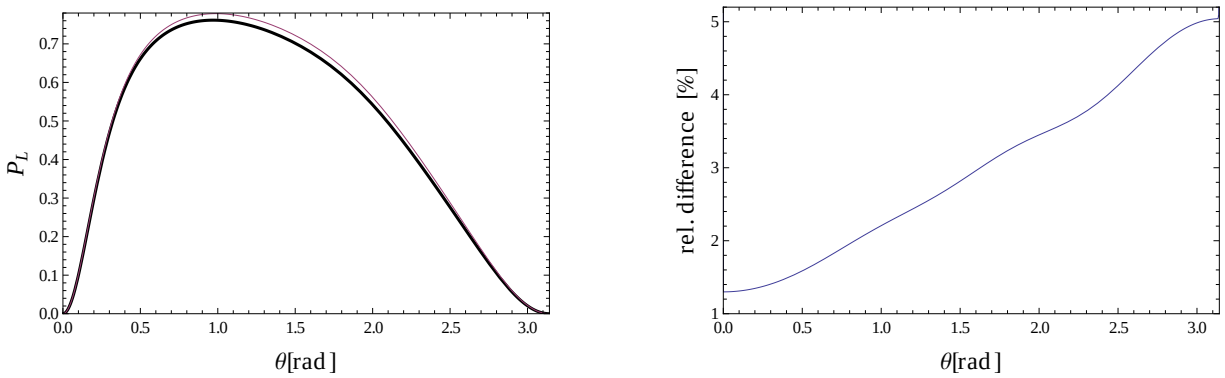

Figure 5.14: Degree of linear polarisation calculated with interpolated polarisation coefficients (red) and relative aberration (blue, right) in comparison to the exact calculations (black) for $Z = 60$ and $\varepsilon_i = 100\,\text{keV}$. The interpolation was done lineary between $Z = 55$ and $Z = 65$. For the denomiator of P_L 4.2.4 the exact calculations were used.

An example table for the polarisation coefficients is given in Tab. 5.4.

Table 5.2: Example table for the polarisation coefficients with $\varepsilon_i = 100\,\text{keV}$, $\varepsilon_f = 1\,\text{eV}$, $Z = 79$ and $\boldsymbol{P} = (0,1,0)$

b	β	$C_{b\beta}^{(P)}$	b	β	$C_{b\beta}^{(P)}$
0	0	0.0455307391400606	7	0	0.000285856828793634
0	1	0	7	1	−0.000364764779191585
0	2	0	7	2	$-2.40240651305769 \times 10^{-6}$
1	0	0.0441582640164469	8	0	0.00230427132754759
1	1	0.00171185670984908	8	1	−0.000142935235599257
1	2	0	8	2	$-2.85733890752573 \times 10^{-6}$
2	0	0.00855567848182772	9	0	0.00228665317019291
2	1	0.00275389471308775	9	1	$-1.6902607985175 \times 10^{-5}$
2	2	−0.000162569058000416	9	2	$-2.00942284462305 \times 10^{-6}$
3	0	−0.017586797529351	10	0	0.00159682781932193
3	1	0.0017361631014266	10	1	$2.54768435832555 \times 10^{-5}$
3	2	$-3.44314808127355 \times 10^{-5}$	10	2	$-6.85234397908418 \times 10^{-7}$
4	0	−0.0218522572947285	11	0	0.000928140484321267
4	1	$8.6291860819548 \times 10^{-5}$	11	1	$2.87155059171829 \times 10^{-5}$
4	2	$4.05234499237739 \times 10^{-5}$	11	2	$-1.79741910964935 \times 10^{-7}$
5	0	−0.014125042213156	12	0	0.000474722184523412
5	1	−0.000633549570957712	12	1	$2.04209268997743 \times 10^{-5}$
5	2	$2.35546154627662 \times 10^{-5}$	12	2	$2.39609107540404 \times 10^{-8}$
6	0	−0.00523617311714304	13	0	0.000219089487156156
6	1	−0.000612430493532175	13	1	$1.17554781622265 \times 10^{-5}$
6	2	$3.55984027972872 \times 10^{-6}$	13	2	$7.78387368883518 \times 10^{-8}$

6 Summary and Outlook

In this work two methods for the description of atomic bremsstrahlung were discussed. The density matrix of the system after the scattering process was derived using a Rayleigh expansion of the photon interaction operator and a partial wave expansion of the free dirac electron. These derivations were done following Yerokhin and Surzhykov [6] as well as Tseng and Pratt [7]. From these results a new parametrisation of two observables of electron-atom bremsstrahlung was presented which expresses the angular distribution and the degree of linear polarisation in terms of spherical harmonics. That means once the coefficients are calculated the calculation of the bremsstrahlung properties is orders of magnitude faster than the calculations after Yerokhin and Surzhykov [6]. Also almost real-time calculations are possible when the tabulated coefficients are used. The coefficients yield a couple of symmetry relations and converge very fast against zero which reduces the needed expansion order remarkably. Also they behave very smooth when the other parameters (nuclear charge, ε_i) are changed so we can get the coefficients for arbitrary parameter sets from an interpolation on a two dimensional grid. The number of coefficients needed increases with the photon energy but does not exceed 50 for energies up to several hundred keV while for energies less than 100 keV for most applications a monadic number of coefficients is enough. Additionally the distance between the nodes on the grid can be increased for higher energies because the coefficients vary less for higher energies so less sets of coefficients are necessary to achieve the same accuracy.

There are some issues to be done on the parametrisation topic in the future. At the moment the interpolation is done lineary. A more fitting basis set for an interpolation would on the one hand increase the accuracy and would allow us on the other hand to increase the distance between the nodes. Furthermore the case should be considered when the electron only partially loses its energy id est $\frac{k}{\varepsilon_i} \neq 1$. This would add one dimension to the interpolation grid. Nevertheless this extension of the method should be easily possible since one would expect the coefficients to have similar properties to the cases discussed in this work for the final electron energy ε_f being changed. Once this is done a way should be found to provide the coefficients in a way which would allow other people to easily access bremsstrahlung properties. Especially for energies less than 1 MeV this can be done in form of tables. For higher energies the tables might become unclear. A way to solve this problem could be a software wich generates coefficient tables for arbitrary parameter sets based on interpolations between hard coded coefficient tables. Also source code, similar to the code used for the calculations in this work, could be made available to be included in existing simulation codes.

Bibliography

[1] V. Balashov, A. Grum-Grzhimailo, and N. Kabachnik, *Polarization and Correlation Phenomena in Atomic Collisions: A Practical Theory Course* (Springer, 2000).

[2] M. Rose, *Elementary Theory of Angular Momentum* (DOVER PUBN Incorporated, 1995).

[3] J. Eichler and W. Meyerhof, *Relativistic atomic collisions* (Academic Press, 1995).

[4] A. Jeffrey and D. Zwillinger, *Table of Integrals, Series, and Products*Table of Integrals, Series, and Products Series (Elsevier Science, 2007).

[5] C. M. Vincent and H. T. Fortune, Phys. Rev. C **2**, 782 (1970).

[6] V. A. Yerokhin and A. Surzhykov, Phys. Rev. A **82** (2010).

[7] H. K. Tseng and R. H. Pratt, Phys. Rev. A **3**, 100 (1971).

List of Figures

List of Tables